Dalton Transactions

ROYAL SOCIETY OF CHEMISTRY

PAPER

View Article Online
View Journal | View Issue

Check for updates

Cite this: *Dalton Trans.*, 2022, **51**, 927

Avoiding water reservoir effects in ALD of functional complex alkali oxides by using O_3 as the oxygen source†

Henrik H. Sønsteby, *[a] Veronica A.-L. K. Killi,[a] Linn M. Rykkje,[a] Justin R. Bickford,[b] Eric G. Martin,[b] Robert C. Hoffman[b] and Ola Nilsen *[a]

Received 23rd November 2021,
Accepted 14th December 2021

DOI: 10.1039/d1dt03960a

rsc.li/dalton

Toxic Pb-containing piezo-, pyro- and ferroelectrics continue to dominate the market even though they were banned from use in consumer products more than a decade ago. There is a strong need for sustainable alternatives, but the lack of facile synthesis routes for thin films exhibiting suitable functional properties have limited the transition from Pb workhorse materials like $Pb(Zr,Ti)O_3$ and $Pb(Mg,Nb)O_3$ – $PbTiO_3$. Atomic layer deposition has proven capable of the deposition of possible successors, such as $LiNbO_3$, $(K,Na)NbO_3$ and $K(Ta,Nb)O_3$, albeit with limited control due to water reservoir effects resulting from the hygroscopicity of intermediate products. In this article, we show that replacing H_2O with O_3 in the deposition of complex alkali oxides provides an alternative and much more controlled process. We exemplify this by deposition of crystalline $K(Ta,Nb)O_3$ with high compositional control and over a larger composition range than previously reported. This opens new doors to a simplified synthesis of polar functional lead-free alternatives.

Introduction

Piezo-, pyro- and ferroelectric materials are essential in modern world technology and constitute a multibillion US$ market. They find frequent use in sensors, actuators, transducers and power generators, and in more exotic technology devices such as non-volatile memory and electro-optics. Unfortunately, the major workhorse materials in current use typically contain lead (Pb), which is a potent environmental pollutant and acutely toxic to most life on earth. Although lead recycling is efficient and exposure from consumer products is kept at a minimum, lead mining continues to be a concern for workers, especially in developing countries. As a result, large economies such as the European Union and the Unites States enforce bans on use of lead in consumer products. The challenge is that synthesis of replacement materials is essentially non-existent, and thus exemptions from the bans are necessary until a new material technology is in place. This has resulted in a surge of effort to develop new, sustainable polar materials that can reduce or eliminate the use of lead.

Alkali metal containing complex oxide perovskites is one family of materials that is predicted to challenge its lead-containing counterparts. Examples like $(K,Na)NbO_3$ (KNN) and $K(Ta,Nb)O_3$ (KTN) exhibit the desired functional properties for a range of applications within sensing, actuation and electro-optics.[1–3] The challenge for both of these compounds is the lack of straightforward methods to deposit high quality crystals and/or thin films. Bulk crystal growth is slow, ineffective, and with unavoidable, large composition gradients throughout the resulting boule, limiting useful implementation in devices.[3–6] Thin film techniques such as sol–gel methods, pulsed laser deposition (PLD) and metalorganic chemical vapor deposition (MOCVD) are also employed, but with severe limitations on device integration due to high-temperature processing or lack of uniformity. These films very often exhibit coarse grains, voids and/or inhomogeneous composition over applicable areas.[7–15]

Atomic layer deposition (ALD) is considered a promising technique for device integration of functional materials containing alkali metals, due to low deposition temperature and high conformity of growth. Based on self-limiting saturative surface chemistry, ALD has the potential to work around issues with precursor pre-reactions and non-uniformity.[16] ALD processes for Na- and K-containing compounds were reported in 2014, and have since been expanded to include KNN and KTN, among others.[17–21] The large majority of these processes utilize alkali metal *tert*-butoxides (*e.g.* NaO^tBu or KO^tBu,

[a]*Department of Chemistry, University of Oslo, Blindern, 0315 Oslo, Norway. E-mail: henrik.sonsteby@kjemi.uio.no, ola.nilsen@kjemi.uio.no*
[b]*U.S. Army Research Laboratory, 2800 Powder Mill Rd., Adelphi, Maryland 20783, USA*

†Electronic supplementary information (ESI) available. See DOI: 10.1039/d1dt03960a

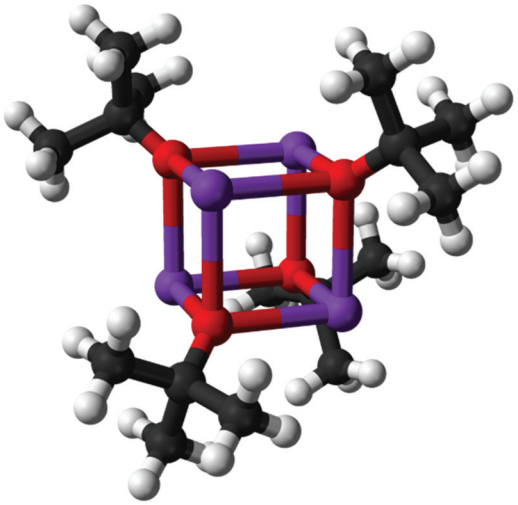

Fig. 1 Tetramer of KO^{t}Bu, the predominant gas phase species of the precursor used.

(Fig. 1)) and water, together with other binary metal process (*e.g.* $Nb(OEt)_5 + H_2O$). While this has proven to provide decent films of *e.g.* KNN and KTN, process control is significantly more difficult than for most ALD routes. This is likely due to a large water reservoir resulting from the hygroscopicity of the intermediary products, such as alkali metal hydroxides.[22] Such effects have been shown to exhibit strong instrumental dependency, meaning that transferring the process between labs or to industry requires significant reoptimization.[23]

Our aim with this work is to remove the reservoir effect to provide a more elegant and reproducible route for deposition of films containing alkali metals.

In traditional metal oxide ALD use of water as a reactant is considered an advantage due to its availability, high vapor pressure and ease of use. For processes with hygroscopic intermediates, however, water as the oxygen source may constitute a silent detrimental factor. Controlling the water dose to precisely a monolayer (saturating) coverage is difficult to achieve reproducibly. Underdosing the water leads to oxidizer deficient growth yielding poor uniformity and a lean growth rate, while overdosing water leads to intermediates that persist from cycle to cycle which act as a water reservoir yielding poor uniformity and excessive growth rate. A pertinent example here is the deposition of $LaAlO_3$, where the binary $Al(CH)_3 + H_2O$ process could not be successfully employed due to formation of $La(OH)_x$, acting as a water reservoir.[24] This was avoided by using O_3 as the oxygen source for both $La(thd)_3$ and $Al(CH)_3$, removing water outright, resulting in a process with high uniformity and reproducibility.

In this article, we use O_3 as an alternative to H_2O as the oxygen source for the deposition of alkali metal containing complex oxides, exemplified by KTN. We show that the group V ethoxides are compatible with O_3, and that there is no water reservoir clouding the growth when including the alkali metal *tert*-butoxides. This provides a much more controlled and reproducible route for deposition of technologically relevant polar materials for sustainable technology.

Experimental

Thin films were deposited in an F-120 Sat ALD reactor (ASM Microchemistry). The deposition temperature was kept at 250 °C under an operating pressure of 2.3 mbar, maintained by 300 cm^3 min^{-1} primary flow rate of N_2. Nitrogen was supplied from gas cylinders (Praxair, 99.999%) and run through a Mykrolis purifier for removal of any oxygen or water contamination. KO^{t}Bu (Aldrich, 97%), $Ta(OEt)_5$ (Sigma-Aldrich, 99%) and $Nb(OEt)_5$ (Sigma-Aldrich, 99%) were used as cation sources, supplied from open boats inside the reactor at 150, 70 and 70 °C, respectively. Fresh KO^{t}Bu was extracted from a container kept inside an argon glovebox for each run. O_3 was used as the oxygen source, supplied from an AC-2505 (In USA) generator fed with O_2 gas (Praxair, >99.5%). The effective upstream gas mixture was 15 wt% O_3 in O_2. 3 × 3 cm^2 Si (100) substrates were used for compositional analysis. Selected films were deposited on cubic perovskite $La_{0.18}Sr_{0.82}Al_{0.59}Ta_{0.41}O_3$ (100) (LSAT, Crystal GmbH) and cubic spinel $MgAl_2O_4$ (100) (MAO, Crystal GmbH) substrates for crystallization.

Post-deposition crystallization was carried out using an OTF-1200X (MTI Corp.) rapid thermal annealing furnace, heating the films to 650 °C In air at a ramp rate of ≈40 °C min^{-1}. The films were subsequently held at 650 °C for 15 minutes, before cooling to room temperature by shutting down the furnace. The samples were extracted at 100 °C after approximately 30 minutes of cooling.

In situ quart crystal microbalance (QCM) investigation was carried out using two 6 MHz AT-cut quartz crystals (Inficon, ∅ = 1.4 cm), mounted approximately 5 cm apart in a holder made in-house. The resonance frequency was monitored by a Colnatec Eon-LT unit and logged with a device made in-house. Variations in surface area of the QCM crystals due to evolution of texture during growth were removed by using internal standards of Nb_2O_5 deposition at even intervals throughout the campaign. These were also used as a basis to convert the signal from Hz to mass per area.

The chemical composition was analyzed using an Axios Max Minerals X-ray fluorescence (XRF) system (Panalytical), equipped with a 4 kW Rh-tube. The system runs using Omnian and Stratos options for standardless measurements of thin films. Routine measurements of thickness on as deposited films were carried out on an alpha-SE spectroscopic ellipsometer (J. A. Woollam) in the 390–900 nm wavelength range. We successfully employed a Cauchy function to model the collected data. X-ray reflectivity (XRR) was used as a complementary method to determine thickness and densities of the Nb_2O_5 internal standards. XRR was carried out on a Panalytical Empyrean diffractometer equipped with a mirror providing parallel CuKα radiation. A proportional point counter was used to detect the reflected beam. X-ray diffraction measurements were carried out on a Bruker AXS D8 Discover

diffractometer equipped with a LynxEye strip detector and a Ge (111) focusing monochromator, providing CuKα_1 radiation.

Results and discussion

A key challenge with alkali metal processes is that the binary alkali metal oxides are not stable in air. A hypothetical KO_x film deposited using KO^tBu and O_3 will immediately react with air upon breaking vacuum, forming hydroxides and/or carbonates. This makes the traditional way of understanding the complex process (*i.e.* combining known binary oxide processes) impractical. As a result, the alkali metal oxide process must be understood as an addition to a single known binary oxide process, such as those for Nb_2O_5 or Ta_2O_5. In the case of KTN, none of the binary oxide processes have been studied in depth using O_3 as the oxygen source. *I.e.*, to understand the growth of the alkali metal oxide, we must first understand the ozone-based processes for Nb_2O_5 and Ta_2O_5.

$Nb(OEt)_5$ + O_3 – an alternative route to Nb_2O_5

Nb_2O_5 is a highly unreactive and passive material that finds use as a dielectric for example in solid electrolyte capacitors. Several ALD processes have been reported for Nb_2O_5, mostly utilizing $Nb(OEt)_5$ or $Nb(N^tBu)(NEt_2)_3$ and water. The former is a well-understood ALD process, described by the following surface reactions:

$$x\ \text{–OH} + \text{Nb(OEt)}_5 \rightarrow \text{–O}_x\text{Nb(OEt)}_{5-x} + x\ \text{EtOH} \quad (1)$$

$$\text{–O}_x\text{Nb(OEt)}_{5-x} + (5-x)\ \text{H}_2\text{O} \rightarrow \text{–O}_x\text{Nb(OH)}_{5-x} + (5-x)\ \text{EtOH} \quad (2)$$

Using O_3 as an oxygen source for growth of Nb_2O_5 with $Nb(OEt)_5$ has, however, remained unexplored until very recently, when Kukli *et al.* utilized O_3 to deposit multilayers of SiO_2 + Nb_2O_5 for use as a switching media.[25,26] This study confirms that the O_3 process provides films with very low hydrogen content, albeit very little is known regarding the mechanism of growth. As a starting point, we confirmed that the process does indeed exhibit self-limiting growth, with a saturation growth-per-cycle (GPC) of 0.40 ± 0.01 Å (ESI Fig. A†). This is very comparable with what we achieved with the water-based process in the same reactor setup, with a GPC of 0.38 ± 0.02 Å.[22]

To uncover the mechanism of growth, we carried out an *in situ* QCM investigation of deposition of pristine Nb_2O_5. O_3 processes are a known clouding factor in QCM experiments due to the exothermic decomposition of O_3. Regardless of that, and by calibrating towards the known average growth of the process and the resulting film density, a close estimate of the mass gain per pulse can be revealed (Fig. 2). Compared to the water-based process, the mass gain during the $Nb(OEt)_5$ pulse is significantly higher.[22] This suggests that the $Nb(OEt)_5$ molecule is coordinating to the surface through activated oxygen from the previous O_3 pulse without significant detachment of ethyl groups. Such detachment takes place during the subsequent O_3 pulse, during which the mass gain drops to 17.6 ng cm^{-2} for the full cycle. This is very comparable to the 16 ng cm^{-2} found for a full water-based cycle, with the slight increase justified by a small increase in density (4.41 *vs.* 4.32 g cm^{-3}) and GPC (0.40 *vs.* 0.38 Å). In conclusion for the $Nb(OEt)_5$ + O_3 process; it forms thin films with growth, control, and quality comparable to the water based process.

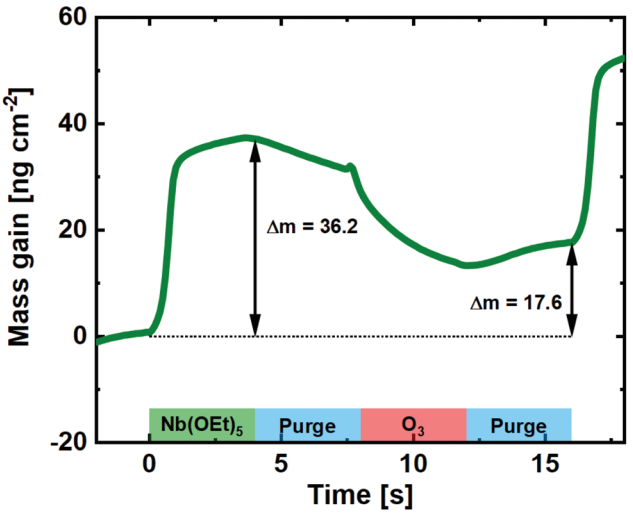

Fig. 2 Mass gain as a function of time for *one* cycle of $Nb(OEt)_5$ + O_3 taken as an average of 100 cycles on a pristine QCM crystal.

$Ta(OEt)_5$ + O_3 – An alternative route to Ta_2O_5

Ta_2O_5 is a high band gap high-k material, finding use in a range of electronics. In ALD it is usually deposited using a $Ta(OEt)_5$ and water, albeit with several other processes reported. The water-based process is well understood, and the mechanism is in agreement with that for its niobium counterpart:

$$x\ \text{–OH} + \text{Ta(OEt)}_5 \rightarrow \text{–O}_x\text{Ta(OEt)}_{5-x} + x\ \text{EtOH} \quad (3)$$

$$\text{–O}_x\text{Ta(OEt)}_{5-x} + (5-x)\ \text{H}_2\text{O} \rightarrow \text{–O}_x\text{Ta(OH)}_{5-x} + (5-x)\ \text{EtOH} \quad (4)$$

The use of O_3 as the oxygen source for reaction with $Ta(OEt)_5$, however, has not been reported in the literature. It is expected to behave very similar to its Nb counterpart, due to the similarity in chemistry and precursor structure. A QCM experiment was carried out for comparison (Fig. 3), and the basic shape of the reaction mass gain is, as expected, very similar to that of $Nb(OEt)_5$ + O_3. The major difference lies in the higher mass gain on the $Ta(OEt)_5$ pulse, which is expected given the much heavier metal ion.

From the GPC of the $Ta(OEt)_5$ + O_3 process (0.50 ± 0.02 Å) and the density of the resulting Ta_2O_5 film (7.82 g cm^{-3}), the average mass gain per cycle is found to be 39.1 ng cm^{-2}.

The mass increase on $Ta(OEt)_5$ pulses is the 66.3 ng cm^{-2}, a factor of 1.83 higher than for the Nb process. This is slightly more than expected when taking the molar masses of the ethoxides into account (406 g mol^{-1} for $Ta(OEt)_5$ *vs.* 318 g mol^{-1}

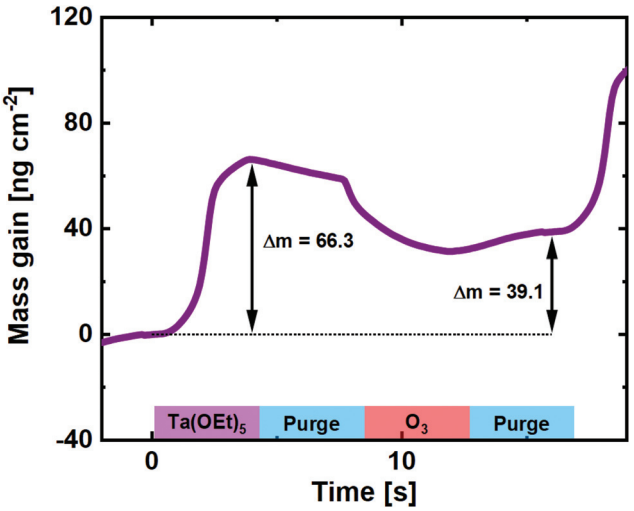

Fig. 3 Mass gain as a function of time for *one* cycle of $Ta(OEt)_5$ + O_3 taken as an average of 100 cycles on a pristine QCM crystal.

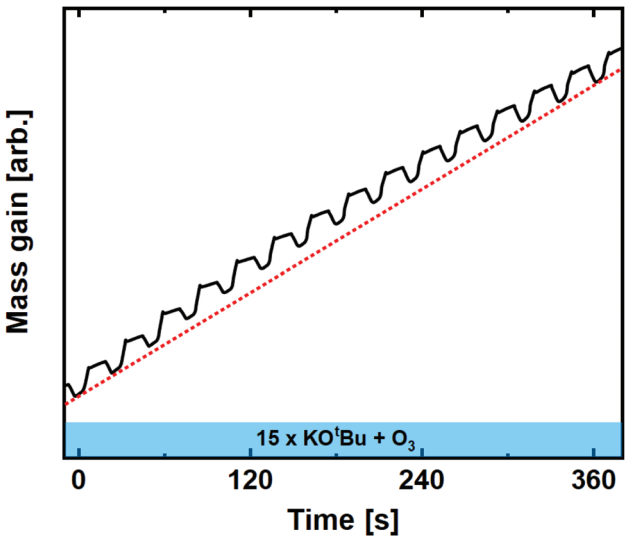

Fig. 4 Mass gain as a function of time for 15 subsequent cycles of KO^tBu + O_3 compared to linear average (dashed red line).

for $Nb(OEt)_5$). This indicates either a higher concentration of adsorbed molecules or fewer ethyl groups detached during Ta $(OEt)_5$ pulsing. The first is made probable by a 30% higher GPC for binary Ta_2O_5, but is likely accompanied also by reduced detachment of ethyl groups. This also explains the relative higher mass drop upon pulsing ozone.

Introducing potassium – higher compositional control

With confirmation that both $Nb(OEt)_5$ and $Ta(OEt)_5$ form compatible processes with O_3, potassium can be included in the mix in the form of KO^tBu. Note here that the pure KO^tBu + O_3 process was tested and seemed to form relatively uniform films before breaking vacuum. At that point it immediately reacts with air, forming a gel-like substance that is likely a mixture of KOH and K_2CO_3. These samples were very impractical to handle, but clearly proved that the KO^tBu + O_3 process provides growth.

Although the KO^tBu + O_3 process is difficult to explore *ex situ*, we carried out an *in situ* QCM linearity test to see whether it is significantly different from the water-based process. As previously reported, the KO^tBu + H_2O process exhibits diverging growth for repeated cycles without passivation, as it acts as a water reservoir that allows KO^tBu to react uncontrolled.[22] The ozone-based process, however, does not exhibit this feature, and remains remarkably linear upon subsequent cycling (Fig. 4). To further compare with the water-based process, we investigated the growth of the K–Nb–O process for different ratios of the binary processes; 1 : 1, 1 : 3 and 1 : 5 (K : Nb).

These were chosen to comply with previous reports for the water-based process in which 1 : 5 was the only ratio that enabled controlled growth.[22] For the water-based process, we observed an extremely high mass gain upon pulsing KO^tBu, which can only be explained by reaction with a water reservoir.[22] The ozone-based process deviates significantly from this observation, showing no signs of uncontrolled growth at any pulsed ratio.

For the 1 : 5 pulsed ratio, we observe that the $Nb(OEt)_5$ + O_3 cycles are similar to what is found for growth of pure Nb_2O_5 (Fig. 5). The average mass gain per-cycle is found to be 17.4 ng cm^{-2}.

We also observe that the single KO^tBu + O_3 cycle behaves very similar compared to that of repeated cycles, however, with a significantly lower mass gain response. Note here that the overall mass gain for a KO^tBu + H_2O cycle with the same K : Nb ratio was previously reported to be as high as 116 ng cm^{-2}, a factor of 20 higher than what is observed in the ozone-based process, likely due to an overdose of water that is hard to control.[22] The control that the O_3 offers is important, as this

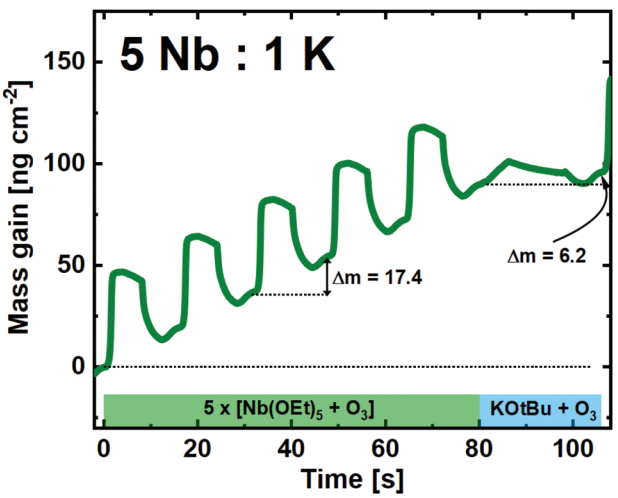

Fig. 5 QCM campaign for a supercycle of 5 : 1 (Nb : K), showing the mass gain per time for the unique subcycles.

will open for a much higher regulation of the overall K : Nb composition in the resulting films.

A similar trend was seen for the 1 : 3 pulsed ratio (ESI Fig. B†), albeit with a notably higher mass gain (25.8 ng cm^{-2}) for the KO^{t}Bu + O_3 cycle. It is probable that this is an effect of the number of preceding $Nb(OEt)_5$ + O_3 cycles, as a pristine Nb_2O_5 surface seems to slow down the growth of KO_x. Interestingly, the 1 : 1 pulsed ratio continued to show remarkably linear and stable growth (Fig. 6). Although the shape of the single $Nb(OEt)_5$ + O_3 cycle is slightly altered compared to growth of pure Nb_2O_5, the overall mass gain is comparable. The KO^{t}Bu + O_3 cycle is very similar to what was observed in the linearity test (Fig. 4), and the overall growth remains linear in nature. It is important to remember that a mass gain of 20.6 ng cm^{-2} for the KO^{t}Bu + O_3 cycle is still quite high taking the molar mass and density of potassium oxide into account. If we hypothesize that the intermediary product of a KO^{t}Bu + O_3 cycle is K_2O; the molar gain of K for such a cycle will still be ≈3.3 times higher than for Nb. This is likely to be an effect of the cubane-like shape of the potassium precursor that allows a large molar concentration of K-ions to be adsorbed on the surface. The advantage here lies in the possibility of finer control compared to the water-based process that led to an extreme and uncontrolled amount of K to be incorporated in the sample.[22]

Towards K(Ta,Nb)O_3 – finer composition control

Lower potassium incorporation per cycle and non-existent reservoir effects for succeeding cycles should in principle lead to higher control of composition in complex systems. To explore this, we turned to one of the more challenging and functionally interesting compounds that includes potassium and group V metals: K(Ta,Nb)O_3. This system adds an additional complexity factor, being a quaternary system where the relative ratio of all three cations is important. In principle, two major ratios are crucial:

1. The K:(Ta + Nb) ratio, which needs to be as close to 1 as possible to achieve growth of perovskite KTN.

2. The Ta : Nb ratio, affecting the Curie temperature of the paralectric → ferroelectric phase transition.

We have previously shown that KTN can be viewed as a *pseudo*ternary system, due to the similarity of growth for Nb $(OEt)_5$ and $Ta(OEt)_5$. These can be interchanged in the complex process to tune the relative Ta : Nb-ratio, without affecting the K:(Ta + Nb) ratio significantly. Hence, the goal with this study was to achieve a finer control of the K-content by using the new ozone based route. To explore this, we deposited a range of samples where the relative ratio of pulsed KO^{t}Bu with respect to the other metal precursors ranged from 16.7 to 50% (Fig. 7). Note that a 50% pulsed ratio of K in the water-based system led to films with very low uniformity and strong composition gradients, degrading immediately in air.[22]

In the ozone-based system, we observe a large initial incorporation of K, which is expected due to the high molar gain of K during a KO^{t}Bu pulse. This can again be explained by the high K-density cubane like shape of the precursor.

However, after the initial increase, we observe a close to linear trend as a function of pulsed KO^{t}Bu. This allows us to directly tune the stoichiometric KTN composition, which is achieved at a 2 : 3 pulsed K:(Ta + Nb) ratio. The films are highly uniform, and with no observed composition gradients over our 7 × 5 cm^2 substrate as mapped by ellipsometry. Also note that changing the relative Ta : Nb ratio does not drastically change the overall composition. For such a quaternary process, we use the shorthand notation (#K – #Ta – #Nb) where the #-symbols note the number of each metal cycles in the overall supercycle. This notation does not represent the individual pulsing sequence. In this work we have arranged the

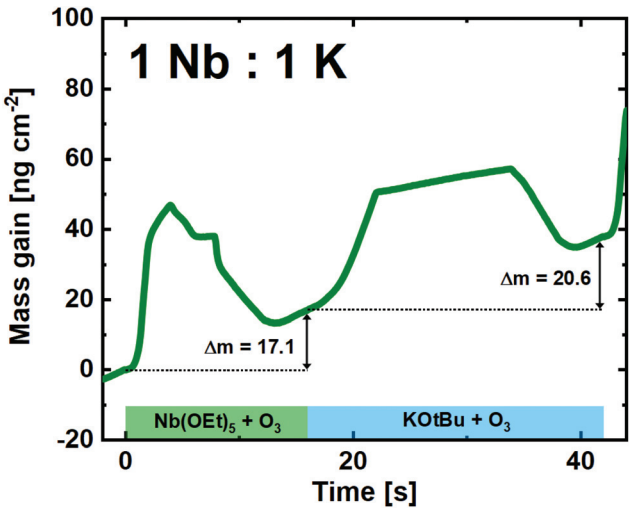

Fig. 6 QCM campaign for a supercycle of 1 : 1 (Nb : K), showing the mass gain per time for the unique subcycles.

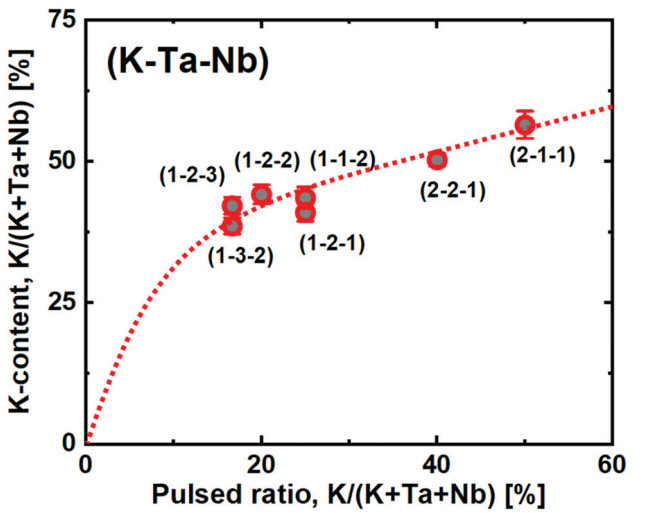

Fig. 7 Potassium content as a function of the pulsed ratio of KO^{t}Bu, showing rapid K-incorporation at low ratios before responding linearly. Dashed red line is a guide of eye, error bars are based on reported confidence in XRF measurements.

pulses to maximize a mixing of the elements. Hence a (2 − 2 − 1) process was arranged as [K + Ta + K + Nb + Ta] to enable an as homogeneous mixture of the cation constituents as possible.

This sample resulted in a composition of $KTa_{0.67}Nb_{0.35}O_3$, which is right in the sweet spot for obtaining a Curie temperature close to room temperature; important for maximizing the electro-optical Kerr coefficient, which is strongest close to the morphotropic phase boundary between the *para-* and ferroelectric states.[27]

Another interesting observation is the close to linear relationship between the film refractive index and K incorporation (Fig. 8), as measured by spectroscopic ellipsometry. Increased potassium content decreases the refractive index, which provides a route for quick identification of approximate K-incorporation for a given Ta : Nb-ratio.

Crystal quality – major improvement

The functionality of polar materials is closely linked to the structure, hence, it is important to obtain the best possible crystallographic integrity. This is especially true for materials applicable in electro-optics, where structural defects alter optical properties.

When deposited using the water based route, KTN exhibited a strong tendency to form unwanted pyrochlore, or a mixed pyrochlore-perovskite phase.[20] The pyrochlore structure, $K_2(Ta, Nb)_2O_6$, does not exhibit the useful electro-optic properties.

With higher control of the cation composition and less water stored in the films, we expected a better crystal quality, *i.e.* phase-pure KTN perovskite. To investigate this, we deposited a series of (2 − 2 − 1) samples with composition $KTa_{0.67}Nb_{0.35}O_3$ on LSAT (100) and MAO (100). These substrates provide different strain scenarios and are both optimal in optical applications due to low interaction with visible light.

MAO adopts a cubic spinel structure with a = 8.089 Å, providing a surface lattice with a_s = 4.045 Å that is slightly larger, but close to the cubic perovskite lattice of KTN ($a \approx 3.98$ Å). LSAT is a cubic mixed perovskite with a = 3.868 Å, imposing compressive strain.

All films were found to be amorphous as deposited, and required post deposition annealing to crystallize. The films were subsequently annealed at 650 °C, where major differences between the film-substrate systems were observed.

On LSAT (100), KTN adopts strong out-of-plane (100) orientation with a *c*-axis cell parameter of 3.987 Å ($2\theta_{(200)}$ = 45.46°, Fig. 9). Being slightly compressed in-plane by the substrate, this *c*-axis elongation is expected. No secondary orientation or traces of other phases were observed, including that of the unwanted pyrochlore phase. The films are also found to be transparent to visible light upon inspection, which can be advantageous for electro-optical applications.

It is evident that the films deposited with the ozone process provide a far superior starting-point for solid phase epitaxy compared to what was seen for the water-based process.[20] Note here that the compressive strain imposed by the LSAT substrate is ≈−3%.This becomes important when comparing it to what is observed on spinel MAO (100). In principle, the tensile strain imposed by MAO (100) on KTN is ≈1.4%, which should be more tolerable than on LSAT. The (100) surface oxygen lattice is similar for the two substrates apart from a small buckling in the O–Al–O bonds that distort the surface of MAO (100) (and the slightly larger O–O-distance in MAO).

Films on MAO are still amorphous as deposited. Upon annealing, however, we observe that while it does exhibit a minor preference for growth in the (100)-direction based on higher intensities for this family of reflections, it is effectively polycrystalline with all allowed reflections visible (Fig. 10).

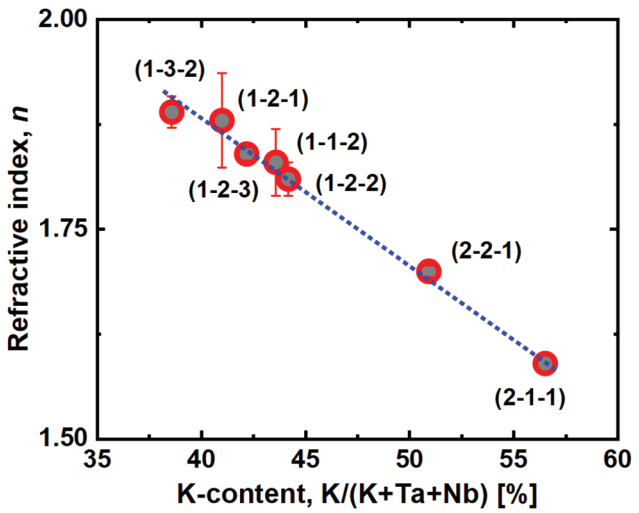

Fig. 8 Refractive index, *n*, as a function of the film potassium cation content. The blue dashed line is a linear fit of the measured data.

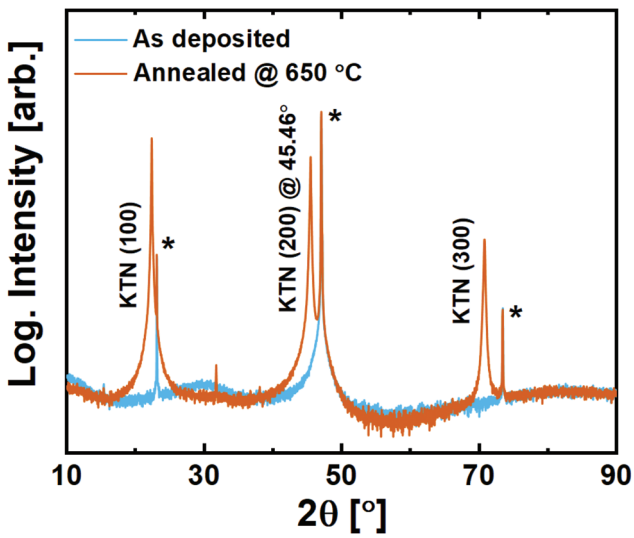

Fig. 9 X-ray diffraction of 200 nm $KTa_{0.67}Nb_{0.35}O_3$ thin films deposited on LSAT (100) substrates. Substrate reflections are marked with*.

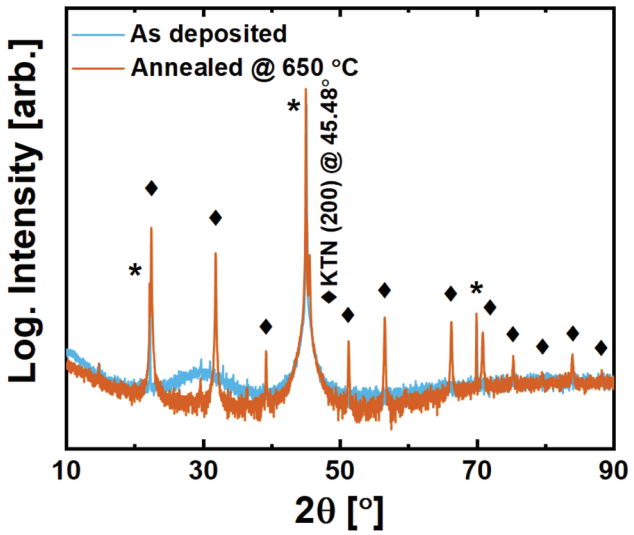

Fig. 10 X-ray diffraction of 200 nm $KTa_{0.67}Nb_{0.35}O_3$ thin films deposited on $MgAl_2O_4$ (100) substrates. Substrate reflections are marked with *, while perovskite film reflections are marked with ◆.

The growth of crystallites upon annealing seems to take place without any template influencing from the substrate. While this close-to random orientation may be challenging in terms of application, it brings an opportunity to investigate the symmetry of the structure. The {110} reflection is not split, and its corresponding plane distance is found to be exactly $a_{KTN}/\sqrt{2}$. This confirms that KTN does indeed adopt the interesting paraelectric cubic phase for the Ta : Nb ratio in question, meaning that the Curie temperature is lower than room temperature. This is important for future application and use of the new reported process.

The random polycrystallinity of KTN deposited on MAO (100) is hypothesized to be an effect of either the O–Al–O bond-buckling present on the MAO (100) surface, or that the KTN structure does not comply with tensile strain, or both. Future work on substrates like $BaTiO_3$, imposing tensile strain without oxygen lattice buckling, could help clarify this question.

We furthermore carried out a Williamson–Hall analysis of the broadening of the reflections, showing that the broadening is predominantly due to particle size and not strain (ESI Fig. C†).

This is as expected in a polycrystalline film sample. In addition, we used the same result to estimate the average minimum crystallite size to be ≈320 nm, which is close to the 380 nm thickness of the as deposited films. The large crystallite size and visually transparent nature of the sample indicates that this still may find application within electro-optics.

Conclusions

Herein, we have shown that replacing the water-based routes for deposition of alkali metal containing complex oxides with novel ozone-based routes significantly enhances process control. A finer composition control is achieved as a result of not having to deal with water reservoir effects throughout growth. We show that the ozone-based routes can be used to deposit high quality alkali metal containing quaternary oxides, exemplified by paraelectric KTN. KTN films can be grown with high compositional control, yielding uniform films with high crystalline quality. The degree of preferred orientation can be tuned by selecting appropriate substrates, ranging from perfectly (100) oriented on LSAT (100) to random polycrystalline on MAO (100).

These ozone-based provide a more elegant growth of alkali metal containing oxides, which may find applications in novel piezo- and ferroelectrics, electro-optics and sodium-/potassium battery technology.

Author contributions

HHS: Conceptualization, data curation, investigation, methodology, supervision, validation, visualization, writing – original draft, writing – review & editing, project administration, funding acquisition. VA-LKK: Data curation, investigation, validation, writing – review and editing. LMR: Data curation, investigation, validation, writing – review and editing. JRB: Conceptualization, investigation, methodology, writing – review and editing. EGM: Investigation, methodology, writing – review and editing. RCH: Conceptualization, investigation, methodology, writing – review and editing. ON: Investigation, supervision, validation, writing – review and editing, project administration, funding acquisition.

Conflicts of interest

There are no conflicts to declare.

Acknowledgements

The authors would like to thank Dr. Nicholas Strnad for fruitful discussions in the infancy of the project.

References

1 J. E. Geusic, S. K. Kurtz, L. G. Van Uitert and S. H. Wemple, *Appl. Phys. Lett.*, 1964, **4**, 141.
2 F. S. Chen, J. E. Geusic, S. K. Kurtz, J. G. Skinner and S. H. Wemple, *J. Appl. Phys.*, 1966, **37**, 388.
3 T. Imai, M. Sasaura, K. Nakamura and K. Fujiura, *NTT Rev.*, 2007, **5**, 1.
4 P. Guenter, *Ferroelectrics*, 1980, **24**, 35.
5 W. A. Bonner, E. F. Dearborn and L. G. Van Uitert, *Ceram. Bull.*, 1965, **44**, 23.
6 D. Rytz and H. J. Scheel, *J. Cryst. Growth*, 1982, **59**, 468.
7 S. Hirano, T. Yogo, K. Kikua, T. Morisihta and Y. Ito, *J. Am. Ceram. Soc.*, 1992, **75**, 1701.

8 J. Burši'k, V. Železný and P. Vaněk, *J. Eur. Ceram. Soc.*, 2004, **24**, 455.
9 S. Yilmaz, T. Venkatesan and R. Gerhard-Multhaupt, *Appl. Phys. Lett.*, 1991, **58**, 2479.
10 A. Rousseau, M. Guilloux-Viry, E. Doghesche, M. Bensalah and D. Remiens, *J. Appl. Phys.*, 2007, **102**, 093106.
11 W. Yang, Z. Zhou, B. Yang, Y. Jiang, H. Tian, D. Gong, H. Sun and W. Chen, *Appl. Surf. Sci.*, 2011, **257**, 7221.
12 C. H. Jung, M. S. Choi, K. S. Lee and D. H. Yoon, *Opt. Mater.*, 2011, **34**, 269.
13 W. Yang, Z. Zhou, B. Yang, Y.- Jiang, Y. Pei, H. Sun and Y. Wang, *Appl. Surf. Sci.*, 2012, **258**, 3986.
14 A. Bouyfasi, M. Mouttalie, V. Demange, B. Gautier, A. Grandfond, S. Députier, S. Ollivier, L'H Hamedi and M. Guilloux-Viry, *Appl. Surf. Sci.*, 2012, **258**, 9297.
15 B. M. Nichols, *"Structural, dielectric, and optical properties of potassium tantalate niobate thin films prepared by metalorganic chemical vapor deposition", dissertation*, Northwestern University, IL, USA, 2000.
16 S. M. George, *Chem. Rev.*, 2010, **110**, 111.
17 E. Østreng, H. H. Sønsteby, S. Øien, O. Nilsen and H. Fjellvåg, *Dalton Trans.*, 2014, **43**, 16666.
18 H. H. Sønsteby, O. Nilsen and H. Fjellvåg, *J. Vac. Sci. Technol., A*, 2016, **34**, 041508.
19 H. H. Sønsteby, O. Nilsen and H. Fjellvåg, *Glob. Chall.*, 2019, **3**, 1800114.
20 J. R. Bickford, H. H. Sønsteby, N. A. Strnad, P. Y. Zavalij and R. C. Hoffman, *J. Vac. Sci. Technol., A*, 2019, **37**, 020904.
21 H. H. Sønsteby, J. E. Bratvold, V. A.-L. K. Killi, D. Choudhury, J. W. Elam, H. Fjellvåg and O. Nilsen, *J. Vac. Sci. Technol., A*, 2020, **38**, 060804.
22 H. H. Sønsteby, V. A.-L. K. Killi, T. A. Storaas, D. Choudhury, J. W. Elam, H. Fjellvåg and O. Nilsen, *Dalton Trans.*, 2020, **49**, 13233.
23 H. H. Sønsteby, A. Yanguas-Gil and J. W. Elam, *J. Vac. Sci. Technol., A*, 2020, **38**, 020804.
24 H. H. Sønsteby, E. Østreng, H. Fjellvåg and O. Nilsen, *Thin Solid Films*, 2014, **550**, 90.
25 K. Kukli, M. Kemell, M. J. Heikkilä, H. Castán, S. Dueñas, K. Mizohata, M. Ritala and M. Leskelä, *Nanotechnology*, 2020, **31**, 195713.
26 K. Kukli, M. Ritala and M. Leskelä, *J. Electrochem. Soc.*, 1995, **142**, 1670.
27 S. Triebwasser, *Phys. Rev.*, 1959, **114**, 63.